Available online at www.sciencedirect.com
ScienceDirect
International Journal of Thermal Sciences 46 (2007) 540–550
International Journal of Thermal Sciences
www.elsevier.com/locate/ijts

Mixed convection in a vertical double pipe heat exchanger

I. Voicu [a,c], T. Maré [a], N. Galanis [b,*], J. Miriel [a], I. Colda [c]

[a] *Laboratoire GCGM, INSA Rennes, 20 Av. Buttes des Coësmes, CS 14315, 35043 Rennes cedex, France*
[b] *Génie mécanique, Université de Sherbrooke, Sherbrooke, Qc, Canada J1K 2R1*
[c] *Facultatea de Instalatii, UTCB, 66 Blv. Pache Protopopescu, cod 73232, Bucuresti, Romania*

Received 3 February 2006; received in revised form 28 July 2006; accepted 5 August 2006

Available online 18 September 2006

Abstract

A numerical study of steady state, simultaneously developing, laminar mixed convection in a vertical double pipe heat exchanger has been conducted for upward parallel flow. The model is elliptic and takes into account conduction in the solid walls as well as dissipation in the two streams. The viscosity and the density of the fluids depend on the temperature while all other thermophysical properties are constant. Results have been calculated for fixed inlet temperatures, a Richardson number equal to 1 for the annular space and three different values in the cylinder (4.85, 1 and 0.34). Flow reversal occurs in the warm fluid for $Ri_c \geqslant 1$ and affects significantly the thermal and hydrodynamic fields. In particular, the temperature of the wall separating the two fluids varies considerably in the flow direction despite its high conductivity. The results include temperature and velocity profiles at different cross sections as well as the axial evolution of bulk and wall temperatures, Nusselt numbers and friction factors in the cylinder and the annular region. The effect of Ri_c on the asymptotic values of the Nusselt numbers is analyzed.

Keywords: Double pipe heat exchanger; Mixed convection; Variable properties; Water–ethylene glycol solution; Flow reversal; Conjugated problem

1. Introduction

Confined mixed convection in ducts of different geometries has been studied extensively both experimentally and numerically. Early studies [1–3] for laminar mixed convection in circular ducts established the main differences between such flow fields and the corresponding ones for forced convection. These include the modification of the hydrodynamic field due to the influence of buoyancy which may even lead to flow reversal [4,5] and a substantial change of the Nusselt number in both the developing and fully developed regions [6,7]. Other studies have investigated mixed convection in an annulus [8,9] as well as the effects of axial diffusion [10,11], wall conduction [12,13], duct inclination [14,15] and turbulence [16,17]. A review article by Jackson et al. [18] summarizes the early results pertaining to mixed convection in vertical tubes while a more recent compilation of 329 studies on mixed convection in horizontal flows [19] illustrates the interest and complexity of this research subject.

However, despite this considerable research effort, the literature on confined mixed convection is limited by the fact that all such studies deal with the hydrodynamic and thermal fields in a single fluid with, usually, either uniform temperature or uniform heat flux applied at the solid walls. In particular, mixed convection in heat exchangers, where two fluids are interacting thermally and buoyancy forces can influence both velocity fields have not been studied to the best of our knowledge. Since these two velocity fields affect the temperature distribution in the solid separating the two fluids and the heat flux distribution along this boundary, it is expected that the thermal condition at the interface between the two fluids is problem specific (i.e. it depends on the Reynolds numbers of the two streams, on their temperature difference, etc.). Therefore the results of previous studies of mixed convection in singly or doubly connected ducts obtained with an arbitrary, simple thermal boundary condition at the solid wall separating the two fluids are not necessarily valid for heat exchangers.

The present study has therefore been undertaken to investigate the effects of mixed convection in heat exchangers using a CFD approach. In this paper we present results for the simplest

* Corresponding author.
E-mail address: nicolas.galanis@usherbrooke.ca (N. Galanis).

1290-0729/$ – see front matter
doi:10.1016/j.ijthermalsci.2006.08.001

Nomenclature

c_p	specific heat	$J\,kg^{-1}\,K^{-1}$	
d	diameter	m	
d_h	hydraulic diameter	m	
Gr	Grashoff number, $= \rho_o \beta_o d_h^2 (T_{oc} - T_{oa})/\mu_o$		
k	conductivity	$W\,m^{-1}\,K^{-1}$	
l	length	m	
L	non-dimensional length, $= l/d_1$		
Pr	Prandtl number, $= \mu_o c_{po}/k_o$		
r	radial coordinate	m	
R	non-dimensional radial coordinate, $= r/d_1$		
Re	Reynolds number, $= \rho_o v_o d_h/\mu_o$		
Ri	Richardson number, $= Gr/Re^2$		
T	temperature	K	
V	non-dimensional velocity, $= v_z/v_{zoc}$		
v_z	axial velocity	$m\,s^{-1}$	
v_r	radial velocity	$m\,s^{-1}$	
z	axial coordinate	m	
Z	non-dimensional axial coordinate, $= z/d_1$		

Greek letters

β	expansion coefficient	K^{-1}
μ	dynamic viscosity	$kg\,m^{-1}\,s^{-1}$
ρ	density	$kg\,m^{-3}$
θ	non-dimensional temperature, $= (T - T_{oa})/(T_{oc} - T_{oa})$	

Subscripts

o	inlet
a	annular space
c	internal pipe
cL	centre line
w	wall

configuration, a vertical double pipe heat exchanger with parallel upward flow in the cylinder and annulus. The density and viscosity of the Newtonian fluids are functions of the temperature and the flow fields are modeled with the elliptical forms of the conservation equations. The hot fluid in the central cylinder is subject to an opposing buoyancy force while the cold fluid in the annulus is aided by buoyancy. Results, presented for three different values of the Richardson number in the cylinder, include velocity and temperature profiles as well as the axial evolution of the bulk temperatures, the wall temperature, the Nusselt numbers and the friction factors.

2. Mathematical modeling

2.1. Geometrical configuration

The system under consideration is a simple parallel-flow heat exchanger consisting of two vertical coaxial copper pipes. Fig. 1 shows the geometry and adopted system of coordinates. The length of the heat transfer zone is 2500 diameters (the inside diameter of the smaller pipe is the reference length). It is preceded and followed by adiabatic zones whose lengths are respectively 120 and 1500 diameters. The upstream adiabatic zone is introduced, as suggested by Shah and London [20], to avoid any interference between the uniform inlet boundary conditions and an eventually important upstream diffusion of heat and momentum. The downstream adiabatic zone is introduced to ensure that fully developed hydrodynamic and thermal conditions can be safely imposed at the outlet [21]. The outer surface of the system at d_4 is assumed to be adiabatic.

2.2. Governing equations

The fluid is a water–ethylene glycol 50% solution. It is a Newtonian incompressible fluid whose density and viscosity vary with temperature according to the following relations [22]:

$$\rho = 984.39 + 1.064T - \left(2.67192 \times 10^{-3}\right)T^2 + \left(2.53477 \times 10^{-7}\right)T^3 \tag{1}$$

$$\log\left(\mu \times 10^2\right) = 65.77 - 0.73037T + \left(3.0917 \times 10^{-3}\right)T^2 - \left(5.93326 \times 10^{-6}\right)T^3 + \left(4.30591 \times 10^{-9}\right)T^4 \tag{2}$$

Its specific heat and conductivity are assumed to be constant.

The flow is assumed to be laminar, steady and two-dimensional (all the variables depend only on the radial and axial coordinates and there is no velocity in the circumferential direction). Radial and axial conduction in the copper walls is taken into account; the conductivity of copper is assumed to be constant. With these assumptions the thermo-hydrodynamic evolution is modeled by the following forms of the governing equations for the fluid:

- Conservation of mass:

$$\frac{\partial(\rho v_z)}{\partial z} + \frac{\partial(\rho v_r)}{\partial r} + \frac{\rho v_r}{r} = 0 \tag{3}$$

- Axial and radial momentum:

$$\rho\left(v_r\frac{\partial v_z}{\partial r} + v_z\frac{\partial v_z}{\partial z}\right) = -\rho g - \frac{\partial p}{\partial z} + \frac{2}{3}\frac{\partial}{\partial z}\left[\mu\left(2\frac{\partial v_z}{\partial z} - \frac{\partial v_r}{\partial r} - \frac{v_r}{r}\right)\right] + \frac{\partial}{\partial r}\left[\mu\left(\frac{\partial v_r}{\partial z} + \frac{\partial v_z}{\partial r}\right)\right] + \frac{\mu}{r}\left(\frac{\partial v_r}{\partial z} + \frac{\partial v_z}{\partial r}\right) \tag{4}$$

$$\rho\left(v_r\frac{\partial v_r}{\partial r} + v_z\frac{\partial v_r}{\partial z}\right) = -\frac{\partial p}{\partial r} + \frac{2}{3}\frac{\partial}{\partial r}\left[\mu\left(2\frac{\partial v_r}{\partial r} - \frac{\partial v_z}{\partial z} - \frac{v_r}{r}\right)\right] + \frac{\partial}{\partial z}\left[\mu\left(\frac{\partial v_r}{\partial z} + \frac{\partial v_z}{\partial r}\right)\right] + \frac{2\mu}{r}\left(\frac{\partial v_r}{\partial r} - \frac{v_r}{r}\right) \tag{5}$$

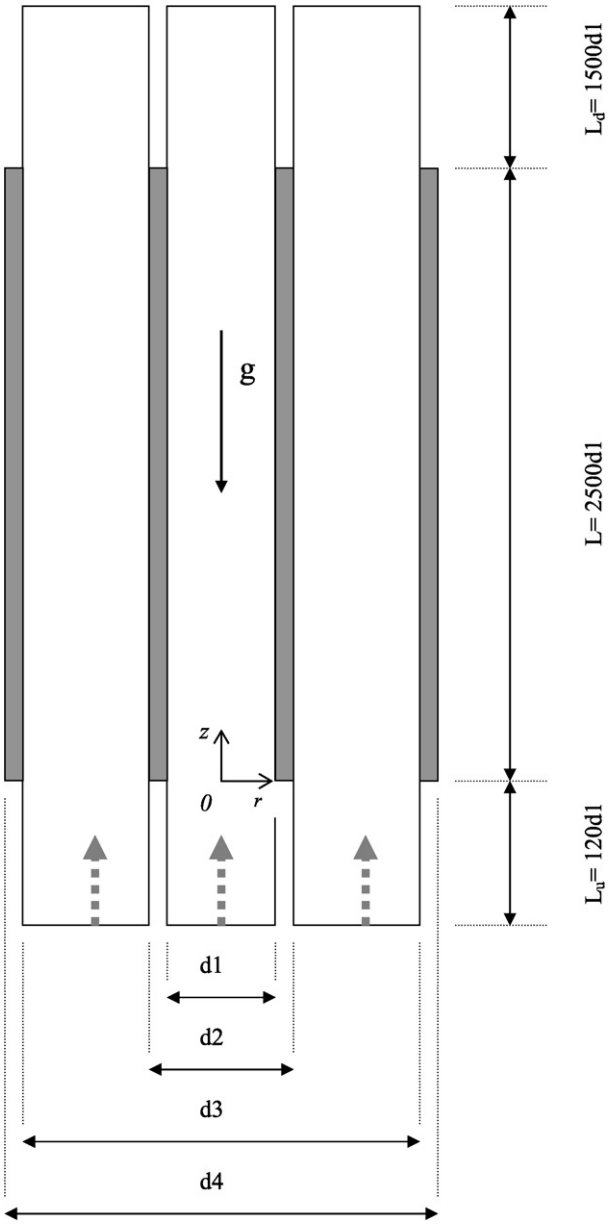

Fig. 1. Geometry and adopted system of coordinates.

- Conservation of energy:

$$k\frac{1}{r}\frac{\partial}{\partial r}\left(r\frac{\partial T}{\partial r}\right)+k\frac{\partial}{\partial z}\left(\frac{\partial T}{\partial z}\right)+\Phi = \rho c_{\mathrm{p}}\left(v_{\mathrm{r}}\frac{\partial T}{\partial r}+v_{\mathrm{z}}\frac{\partial T}{\partial z}\right)-v_{\mathrm{r}}\frac{\partial p}{\partial r}-v_{\mathrm{z}}\frac{\partial p}{\partial z} \tag{6}$$

where

$$\Phi = 2\mu\left[\left(\frac{\partial v_{\mathrm{r}}}{\partial r}\right)^2+\left(\frac{v_{\mathrm{r}}}{r}\right)^2+\left(\frac{\partial v_{\mathrm{z}}}{\partial z}\right)^2+\frac{1}{2}\left(\frac{\partial v_{\mathrm{r}}}{\partial z}+\frac{\partial v_{\mathrm{z}}}{\partial r}\right)-\frac{1}{3}(\nabla q)^2\right] \tag{7}$$

and

$$\nabla q = \frac{\partial v_{\mathrm{r}}}{\partial r}+\frac{\partial vz}{\partial z}+\frac{v_{\mathrm{r}}}{r} \tag{8}$$

For the solid, conservation of energy is expressed by

$$k\frac{1}{r}\frac{\partial}{\partial r}\left(r\frac{\partial T}{\partial r}\right)+k\frac{\partial}{\partial z}\left(\frac{\partial T}{\partial z}\right)=0 \tag{9}$$

Although these partial differential equations cannot be converted into a non-dimensional system due to the complexity of Eqs. (1) and (2), the flow can be characterized uniquely by using non-dimensional parameters evaluated at the inlet conditions. Thus, for the fixed geometry of Fig. 1 and the assumed fluid–solid combination, the flow field depends on the following non-dimensional parameters: the Reynolds and Prandtl numbers in the cylinder and the annulus as well as the two Grashof numbers based on the temperature difference between the two fluid streams at the inlet. Alternatively, the Richardson and Peclet numbers for each system can be used instead of the Reynolds and the Grashof numbers. The expressions of these parameters are specified in the nomenclature.

2.3. Boundary conditions

The fluids are assumed to enter the system at $z=-L_{\mathrm{u}}$ with uniform axial velocities and temperatures. Therefore, for each fluid (indices 'c' and 'a')

$$\text{At } z=-120d_1\text{: } v_{\mathrm{z}}=v_o,\ v_{\mathrm{r}}=0,\ T=T_o \tag{10a}$$

At the outlet from the downstream adiabatic zone it is assumed that both flow fields are fully developed since this zone is very long. Therefore, for both fluids:

$$\text{At } z=L+L_{\mathrm{d}}=4000d_1\text{: } \frac{\partial v_{\mathrm{r}}}{\partial z}=\frac{\partial v_{\mathrm{z}}}{\partial z}=\frac{\partial T}{\partial z}=0 \tag{10b}$$

At the fluid solid interfaces, the non-slip condition as well as the equality of temperature and heat flux is applied. Thus:

$$\text{For } -120d_1\leqslant z\leqslant 4000d_1\text{:}\quad v_{\mathrm{r}}=v_{\mathrm{z}}=0 \text{ at } r=0.5d_1,\ r=0.5d_2 \text{ and } r=0.5d_3 \tag{10c}$$

$$\text{For } 0\leqslant z\leqslant 2500d_1\text{: } T_{\mathrm{c}}=T_{\mathrm{w1}},\ T_{\mathrm{w2}}=T_{\mathrm{a}} \text{ and } T_{\mathrm{a}}=T_{\mathrm{w3}} \text{ at } r=0.5d_1,\ r=0.5d_2 \text{ and } r=0.5d_3 \tag{10d}$$

respectively

$$\text{For } 0\leqslant z\leqslant 2500d_1\text{:}\quad k_{\mathrm{c}}\frac{\partial T_{\mathrm{c}}}{\partial r}=k_{\mathrm{w}}\frac{\partial T_{\mathrm{w}}}{\partial r},\ k_{\mathrm{w}}\frac{\partial T_{\mathrm{w}}}{\partial r}=k_{\mathrm{a}}\frac{\partial T_{\mathrm{a}}}{\partial r},\ k_{\mathrm{a}}\frac{\partial T_{\mathrm{a}}}{\partial r}=k_{\mathrm{w}}\frac{\partial T_{\mathrm{w}}}{\partial r} \text{ at } r=0.5d_1,\ r=0.5d_2 \text{ and } r=0.5d_3 \tag{10e}$$

respectively

$$\text{For } -120d_1\leqslant z\leqslant 0 \text{ and } 2500d_1\leqslant z\leqslant 4000d_1\text{:}\quad \frac{\partial T_{\mathrm{c}}}{\partial r}=\frac{\partial T_{\mathrm{a}}}{\partial r}=0 \text{ at } r=0.5d_1,\ r=0.5d_2 \text{ and } r=0.5d_3 \tag{10f}$$

Finally, at the outside surface of the heat exchanger and at the ends of the solid walls which are assumed to be perfectly insulated:

$$\text{For } 0\leqslant z\leqslant 2500d_1\text{: } \frac{\partial T_{\mathrm{w}}}{\partial r}=0 \text{ at } r=0.5d_4 \tag{10g}$$

$$\text{For } 0.5d_1<r<0.5d_2 \text{ and } 0.5d_3<r<0.5d_4\text{:}\quad \frac{\partial T_{\mathrm{w}}}{\partial r}=0 \text{ at } z=0 \text{ and } z=2500d_1 \tag{10h}$$

3. Numerical solution and code validation

3.1. Numerical procedure

The system of coupled, non-linear, elliptic partial differential equations (3)–(9), subject to their boundary conditions, has been successfully solved by using the numerical method based on the 'finite volume approach' with the aid of software FLUENT [23]. This method, as others of the Simple family, is based on the spatial integration of conservation equations over finite control volumes. A second-order method has been employed throughout to compute the heat and momentum fluxes. The resulting 'discretized equations' have been solved in a sequential manner, using the combination of the efficient multiple-and-alternate-sweeping technique, the 'line-by-line' technique and the standard TDMA ('Three-Diagonal Matrix Algorithm'). On the other hand, the 'pressure correction' equation, obtained by a combination of the discretized form of the Navier–Stokes equations and the continuity equation, has been employed not only to calculate the pressure field but also to correct the assumed velocity field during the calculation process in order to progressively satisfy all the discretized equations. Complete information regarding the numerical method is well documented elsewhere [21,23].

The residuals resulting from the integration of the conservation equations were used as convergence indicators. During the iterative calculation process, these residuals were constantly monitored and scrutinized. For all the simulations performed in this study, converged solutions were usually achieved with residuals as low as 10^{-6} (or less) for all governing equations.

3.2. Discretization grid

In order to ensure the accuracy of the results and their independence with respect to the number of nodes used in the discretization process, several grids were tested. The corresponding predicted velocity and temperature profiles at different axial positions were compared and it was thus established that the $53 \times 14\,800$ non-uniform grid was appropriate for the problem under study. In the radial direction the adopted grid has 22 nodes in the cylindrical space, 2 in the solid between d_1 and d_2, 27 in the annulus and 2 in the solid between d_3 and d_4. In the axial direction it has 300, 11 500 and 3000 respectively in the adiabatic upstream zone, the zone of thermal transfer and the adiabatic downstream zone. The discretization grid is non-uniform in both directions: it is finer near the entrance of the heated tube and near the walls where gradients of velocity and temperature are important.

3.3. Code validation

There exists, to our knowledge, no experimental or analytical detailed information on the axial evolution of the temperatures and velocities for the case of laminar mixed convection in a double pipe heat exchanger. Therefore, our validation was carried out in two steps.

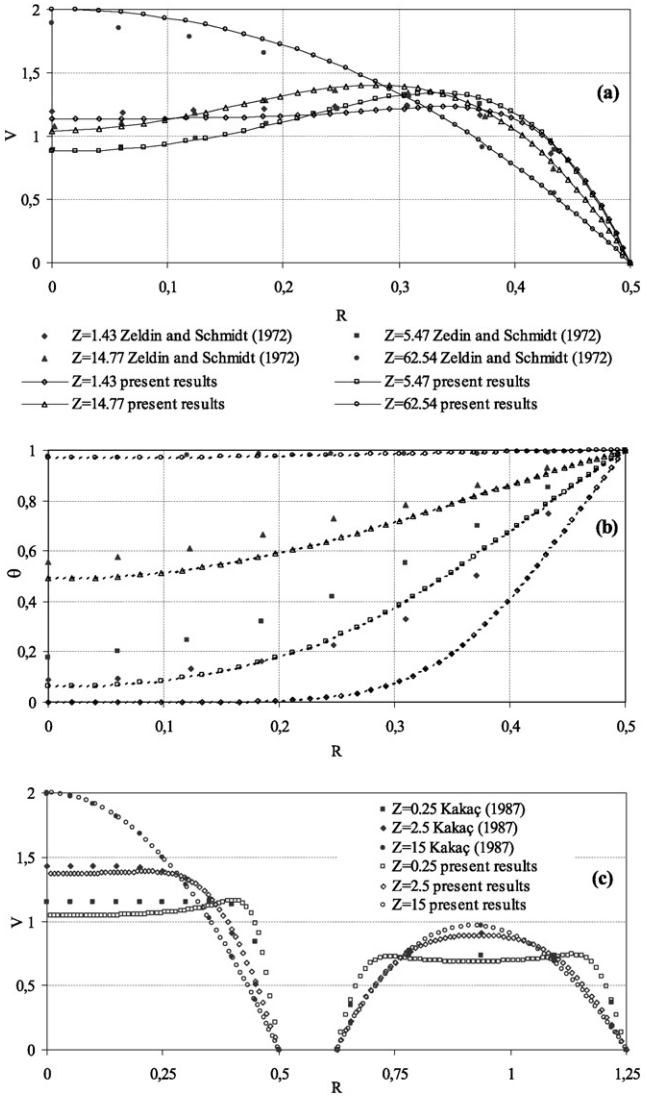

Fig. 2. Validation of numerical results (a), (b) experimental results [3]; (c) analytical solution [24].

(a) A comparison of the experimental results by Zeldin and Schmidt [3] for laminar mixed convection of air in an isothermal vertical pipe with corresponding numerical results shows good agreement for both velocity (Fig. 2(a)) and temperature (Fig. 2(b)) profiles except for the temperature profile near the heating region inlet ($Z < 10$). However, as explained by Zeldin and Schmidt [3] the measured temperatures in that region were influenced by upstream conduction through the walls of the experimental setup. The numerical predictions of their model for these temperature profiles are very close to the corresponding calculated values in Fig. 2(b).

(b) A comparison of the velocity profiles for isothermal flow of water in both cylindrical and annular regimes shows good qualitative agreement (Fig. 2(c)) with corresponding analytical results reported by Kakaç [24]. The numerical results, which illustrate the well-established "overshoot" near the entrance, are believed to be more accurate since

the analytical solutions do not include the effects of axial diffusion.

4. Results and discussion

The results presented in this paper have been calculated for a fixed geometry ($d_2/d_1 = 1.25$, $d_3/d_1 = 2.5$, $d_4/d_1 = 2.75$), for fixed inlet temperatures (313 K for the internal cylinder and 283 K for the annular space), a single Reynolds number equal to 110 for the annulus and three different Reynolds numbers equal to 400, 880 and 1500 for the cylinder. Based on these values the corresponding Grashof numbers are equal to 7.76×10^5 and 1.22×10^4 for the fluid in the cylinder and the annulus respectively while Richardson numbers are equal to 1 for the annular space and 4.85, 1, 0.34 for the cylinder.

Cross sectional averages or bulk variables are calculated using the following expressions:

$$\overline{\rho} = \int_A^B \rho r\,dr \Big/ \int_A^B r\,dr \tag{11}$$

$$\overline{v_z} = \int_A^B \rho v_z r\,dr \Big/ \overline{\rho} \int_A^B r\,dr \tag{12}$$

$$\overline{T} = \int_A^B \rho T v_z r\,dr \Big/ \overline{\rho}\,\overline{v_z} \int_A^B r\,dr \tag{13}$$

with $A = 0$, $B = d_1/2$ for the cylindrical space and $A = d_2/2$, $B = d_3/2$ for the annular space.

4.1. Evolution of velocity and temperature

Figs. 3 and 4 respectively show the non-dimensional velocity and temperature profiles in the cylinder and the annulus at different axial positions for the three cases under consideration. At the entrance of the heat transfer zone ($Z = 0$) the velocity profiles in the cylinder for the two lower values of the corresponding Richardson number ($Ri_c = 0.34$ and $Ri_c = 1$) are parabolic (Poiseuille profile). This implies that upstream diffusion is negligible in these two cases with fairly important mass flow rates (relatively high Reynolds numbers). This result also shows that the length of the upstream adiabatic zone is indeed sufficient to ensure that the flow becomes hydrodynamically developed (in fact, hydrodynamically developed conditions are reached upstream of $Z = 0$ in both these cases). On the other hand, for $Ri_c = 4.85$, a careful examination of the corresponding velocity profile at $Z = 0$ shows significant departures from the parabolic distribution. Near the wall the velocities are lower than those for Poiseuille flow while the opposite is true near the centreline. Since the velocity profile in the upstream adiabatic zone is even in this case parabolic (velocity profiles for $Z < 0$ are not shown here for lack of space), the distortion observed at $Z = 0$ is due to upstream diffusion. This difference from the previous two cases with lower Richardson numbers is due to the fact that the same temperature difference is applied to a much lower mass flow rate. Hence convection is less important and

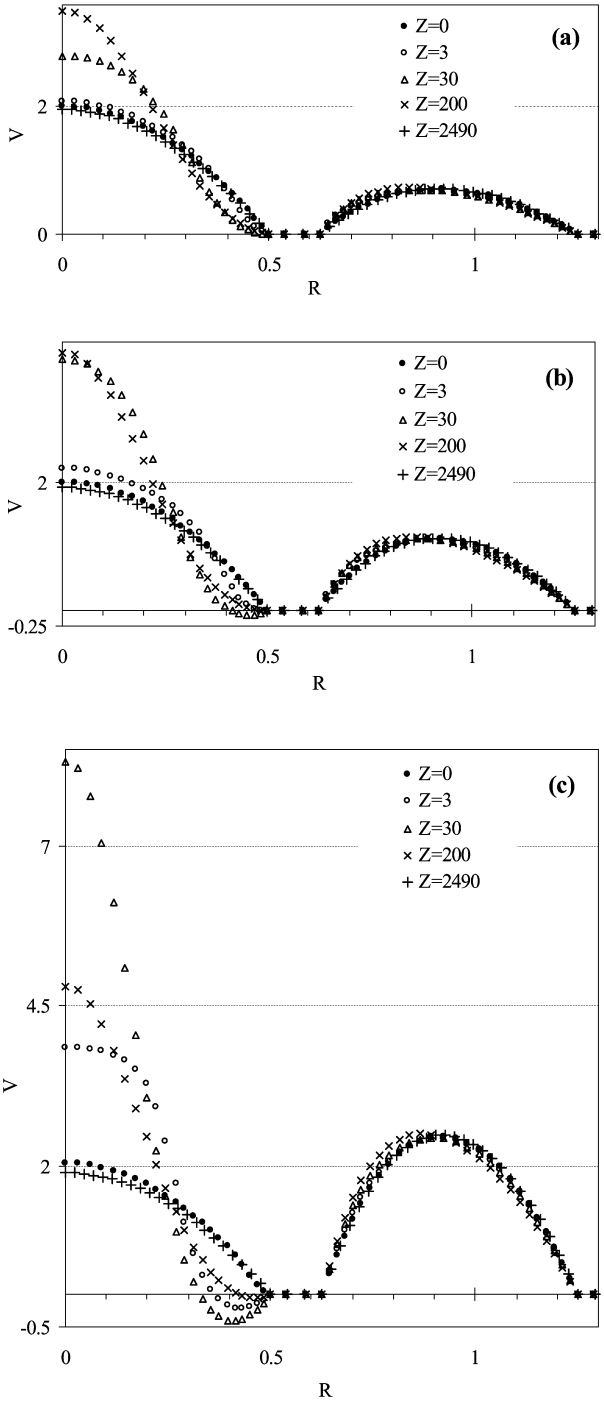

Fig. 3. Non-dimensional velocity profiles at different axial positions ((a) $Ri_c = 0.34$, (b) $Ri_c = 1$, (c) $Ri_c = 4.85$).

conduction more significant when $Ri_c = 4.85$. The fluid in the vicinity of the wall at $Z = 0$ is therefore colder (cf. Fig. 4) and the ensuing buoyancy forces influence the corresponding velocity profile as described above.

Further downstream, as heat transfer becomes important, the temperatures of the two fluids begin to approach each other especially near the cylinder wall (cf. Fig. 4): the warm fluid in that region becomes cooler while the cold fluid warms up. These temperature differences within each stream give rise to

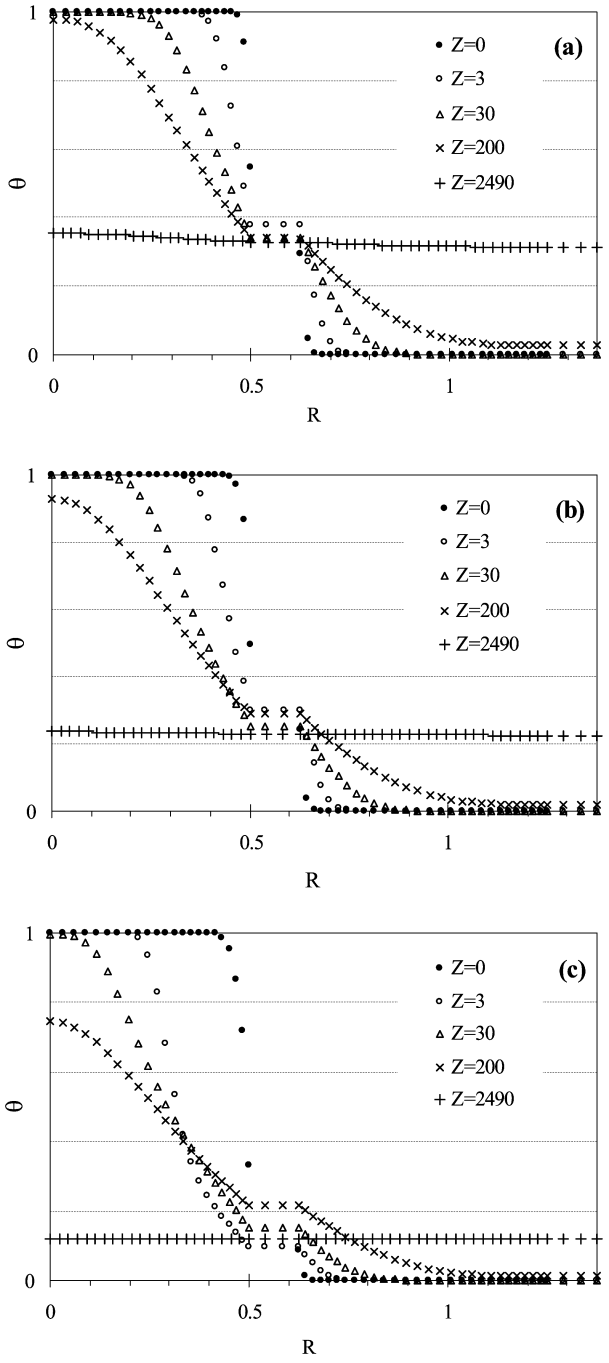

Fig. 4. Non-dimensional temperatures at different axial positions ((a) $Ri_c = 0.34$, (b) $Ri_c = 1$, (c) $Ri_c = 4.85$).

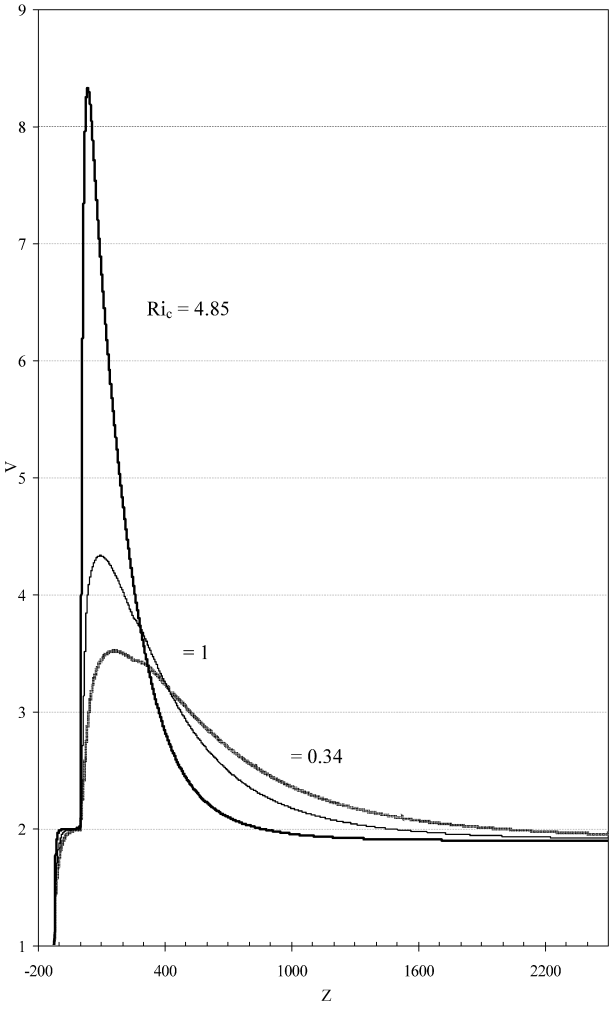

Fig. 5. Axial evolution of centerline velocity.

important buoyancy forces. In the cylinder, the cooler fluid near $R = 0.5$ is subject to a downward buoyancy and it therefore decelerates. As a result, the velocity in the central part of the cylinder increases in order to satisfy continuity. These effects become more important with increasing values of the Richardson number which reflects the relative importance of natural and forced convection. In fact, for $Ri_c = 1$ negative velocities are observed at $Z = 30$ for $0.4 < R < 0.5$. The corresponding maximum velocity at $r = 0$ is almost twice as high as the centreline velocity at $Z = 0$. For $Ri_c = 4.85$ the region of negative velocities is much larger and the maximum non-dimensional velocity at $Z = 30$ is approximately equal to 8.3.

As the two fluids move downstream and approach the end of the heat transfer zone ($Z = 2500$) the temperature tends to become uniform over the entire cross-section ($0 \leqslant R \leqslant d_4/2d_1$). It is numerically very close to the value calculated by applying the first law of thermodynamics to the control volume defined by the following three surfaces: $Z = 0$, $Z = 2500$ and $R = d_4/2d_1$. This equilibrium value is lower for the case with $Ri_c = 4.85$ since in that case the mass flow rate of hot fluid is lowest. Finally it is also obvious that, in accordance with the mass flow ratio between the two streams, the temperature change of the warm fluid is much more important than that of the cold fluid. As a result, the velocity profile in the annulus changes very little (see Fig. 3).

Figure 5 shows in more detail the axial evolution of the centreline velocity for the three cases under consideration. At the system's inlet ($Z = -120$) the velocity profile is uniform for all three cases and therefore $V_{cL,o} = 1$. Then, as the fluid in the cylinder moves along the upstream adiabatic zone the boundary layer grows, the velocity profile approaches the parabolic distribution and V_{cL} becomes equal to 2. In the entry region of the heating zone the buoyancy force is the controlling fac-

tor as explained earlier. The value of V_{cL} increases rapidly and reaches a maximum which increases with the Richardson number of the cylinder flow. The position of this maximum velocity moves closer to $Z = 0$ as this Richardson number increases. Beyond this position the radial temperature difference in the cylinder decreases (cf. Fig. 4) and therefore the influence of the buoyancy force diminishes. Thus the velocity profile tends once again towards the parabolic distribution (cf. Fig. 3). In particular, the negative velocities near the wall at $R = 0.5$ disappear indicating that the zone of flow reversal does not extend to the exit of the heating zone. It is also important to note (see Figs. 3 and 5) that the non-dimensional centreline velocity near the end of the heating zone ($Z = 2490$) is slightly lower than at its inlet ($Z = 0$). However, if the local average velocity (rather than the uniform inlet one) is used to non-dimensionalize the velocity profile at $Z = 2490$, the centreline value is close to 2, the theoretical value for the parabolic profile. This is due to the fact that the average velocity in the cylinder decreases as Z increases since the fluid becomes cooler and its density increases as it moves downstream. The velocity profile at that axial position is closest to the parabolic distribution for $Ri_c = 4.85$ and farthest from this forced convection distribution for $Ri_c = 0.34$. In the latter case, the velocity profile becomes parabolic in the downstream adiabatic zone indicating that in this case the heating length is not sufficient to achieve fully developed conditions. This observation is corroborated by the fact that, for $Ri_c = 0.34$ the radial temperature distribution at $Z = 2490$ is not yet exactly uniform (cf. Fig. 4). This result justifies the inclusion of the downstream adiabatic zone in the calculation domain.

Fig. 6 shows the extent of the region with negative velocities in the R–Z plane (on the left the coordinates for both Z and R are linear, on the right the coordinates for R are linear but those for Z are logarithmic in order to show more clearly the conditions very close to the beginning of the heating zone). The case with $Ri_c = 0.34$ does not appear in these figures since flow reversal does not take place for this case. The results of Fig. 6 clearly show that the extent of the region with negative velocities increases when the Richardson number in the cylinder increases: indeed, flow reversal for $Ri_c = 4.85$ starts closer to the beginning of the heating zone, extends further downstream and its maximum radial dimension is almost twice that corresponding to $Ri_c = 1$. In view of these observations, it is interesting to revisit the temperature profiles in Fig. 4 and examine the temperature of the warm fluid at $R \cong 0.48$. In the case without flow reversal ($Ri_c = 0.34$) this temperature decreases monotonically as Z increases. On the other hand, in the case with flow reversal, this temperature does not vary monotonically with Z. For $Ri_c = 4.85$ in particular, it starts with a high value at $Z = 0$ (in accordance with the imposed inlet conditions), reaches a minimum at $Z = 3$ (which is even lower than the eventual equilibrium temperature at $Z = 2490$) and then increases at $Z = 30$ and even further at $Z = 200$. This behaviour is obviously related to the extent and size of the region with negative velocities. At $Z = 3$, which is very close to the beginning of the region with negative velocities (cf. Fig. 6), the warm fluid in the cylinder is almost stagnant. Therefore, it convects very little thermal energy and its temperature is closer to that of

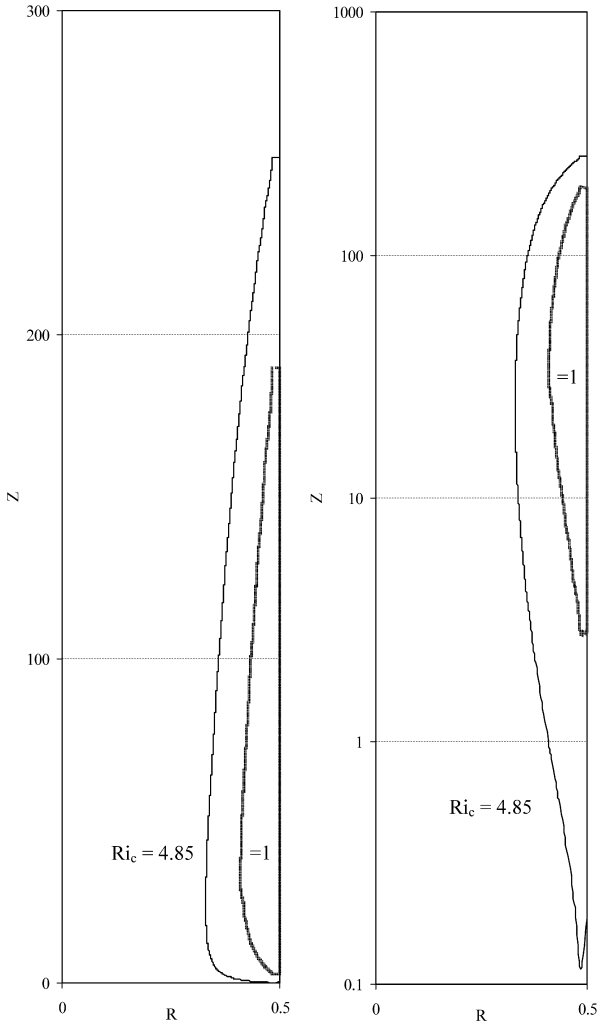

Fig. 6. Limits of negative velocities.

the cold fluid. At $Z = 30$ the negative velocities in the cylinder are fairly important (cf. Fig. 3(c)) and the heat transfer situation near the wall is similar to that prevailing in a counter flow heat exchanger. Thus, the temperature of the warm fluid decreases in the direction of the flow or, equivalently, increases with increasing Z. Beyond $Z \approx 250$, flow reversal has disappeared and the hydrothermal conditions correspond to those in a parallel flow heat exchanger. Hence, the temperature at $R \approx 0.48$ decreases as Z increases beyond this axial position.

Fig. 7 which shows the axial evolution of the fluid bulk temperatures and those of the solid walls provides further evidence of the influence of flow reversal. This becomes obvious by focusing on the temperature of the wall between the two streams of fluid which is almost uniform in the radial direction since the conduction of copper is very high. In all three cases, we observe that the axial gradient of this temperature is zero at the inlet and outlet of the heating region in accordance with the corresponding boundary condition. In the case without flow reversal ($Ri_c = 0.34$) the temperature of this wall initially decreases as Z increases and reaches, within a few diameters a nearly constant value equal to the outlet equilibrium value. In the case with moderate flow reversal ($Ri_c = 1$) this wall tem-

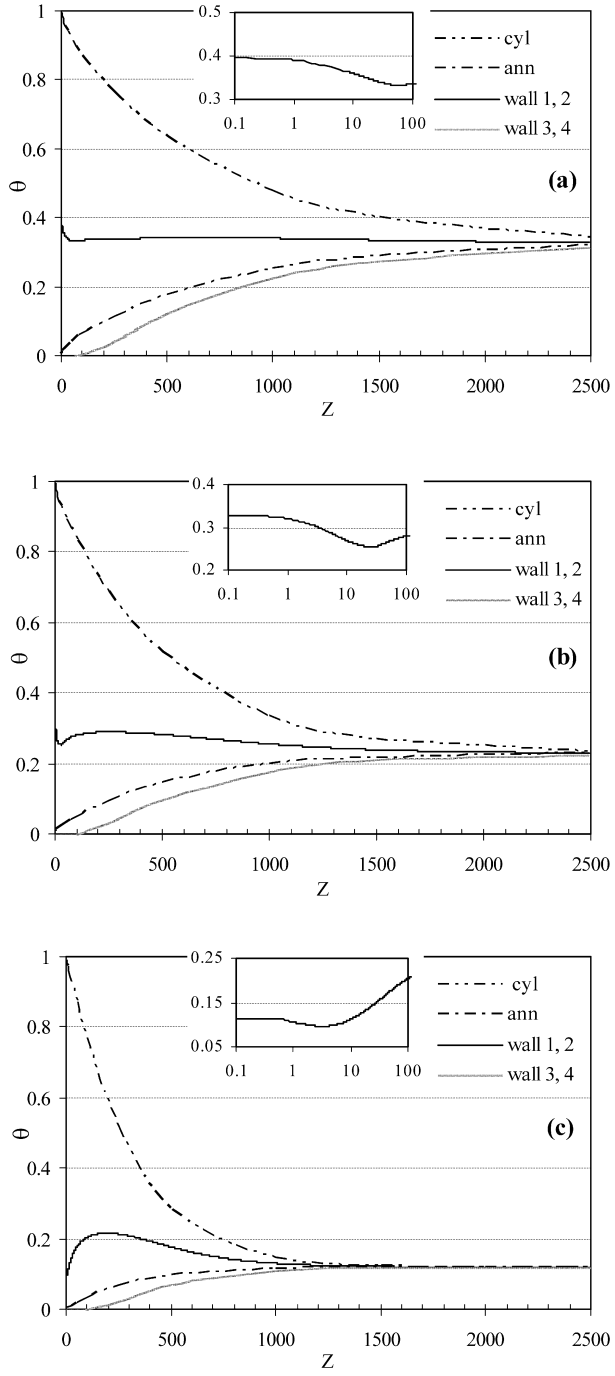

Fig. 7. Axial evolution of the bulk and wall temperatures ((a) $Ri_c = 0.34$, (b) $Ri_c = 1$, (c) $Ri_c = 4.85$).

perature initially decreases, reaches a minimum at $Z = 20.5$ and then increases to a local maximum at $Z = 250$ before decreasing towards the corresponding outlet equilibrium value. In this case, the wall temperature at $Z = 0$ is higher than the local maximum at $Z = 250$. Finally, in the case with important flow reversal ($Ri_c = 4.85$) the qualitative behaviour of this wall temperature is similar to that for the previous case but the local maximum at $Z = 195$ is higher than the value at $Z = 0$. We note that, as Ri_c increases, the position of the local minimum and maximum move upstream while the difference between these two extreme temperatures increases. These temperature distributions obviously indicate that axial heat transfer within this wall is very different for these three cases. The presence of local maximum and minimum values of this temperature also has implications on the strains and thermal stresses for the solid wall.

The axial evolution of the fluid bulk temperatures and outer wall temperature shown in Fig. 7 are more regular and predictable. The outer wall temperature is the lowest and increases towards the outlet equilibrium value more slowly than that of the cold fluid. The warm fluid temperature decreases regularly and is always the highest. The thermal development length decreases as the Richardson number in the cylinder increases.

4.2. Axial evolution of local Nusselt number and friction factor

The local Nusselt number and friction coefficient are calculated from the following expressions:

$$Nu = 2\frac{\partial T}{\partial r}\bigg|_{r=r_w}\left[\frac{\overline{T} - T_w}{d_h}\right]^{-1} \tag{14}$$

and

$$f\,Re = 8\frac{\partial v_z}{\partial r}\bigg|_{r=r_w}\left[\frac{\overline{v_z}}{d_h}\right]^{-1} \tag{15}$$

Their values have been calculated for each of the three fluid-solid interfaces at $r = 0.5d_1$ (wall 1), $r = 0.5d_2$ (wall 2) and $r = 0.5d_3$ (wall 3).

Fig. 8 shows the axial evolution of the local Nusselt numbers for the three cases under consideration. The values for wall 3 are always very small since the outside of the system at $r = 0.5d_4$ is adiabatic. However they are not identically equal to zero since some energy is exchanged between the cold fluid and wall 3 and conducted along the solid. However, for all practical purposes, this effect can be neglected. The values for walls 1 and 2 which control the performance of the heat exchanger are, as expected, very high in the immediate vicinity of $Z = 0$. However, they decrease very rapidly particularly on the warm side (wall 1). As predicted in several studies of mixed convection [5, 7], Nu_1 reaches a minimum which is more pronounced and occurs earlier as the corresponding Richardson number increases. It then increases slightly and reaches an asymptotic value corresponding to fully developed conditions. On the other hand, Nu_2 decreases monotonically towards its asymptotic value in all three cases. Table 1 shows the asymptotic values of Nu_1 and Nu_2 and compares them to the corresponding values for forced convection [24] in isothermal tubes (T) or tubes with uniform heat flux at the solid–fluid interface (H). We notice that, for the three values of Ri_c under consideration, the calculated values of Nu_1 are intermediate between the forced convection values corresponding to the T and H boundary conditions. On the other hand, Nu_2 is always smaller than the forced convection value corresponding to the T condition. Furthermore as Ri_c increases, the calculated values of Nu_1 increase while those of Nu_2 decrease. This intriguing behaviour can be explained by analogy

Table 1
Nusselt number in the fully developed region

	Present results at $Z = 2500$		Forced convection (T)		Forced convection (H)	
	Cylinder wall 1	Annulus wall 2	Cylinder wall 1	Annulus wall 2	Cylinder wall 1	Annulus wall 2
$Ri_c = 0.34$	3.86	5.53	3.657	5.73	4.364	6.181
$Ri_c = 1$	3.88	5.34	3.657	5.73	4.364	6.181
$Ri_c = 4.85$	4.24	4.56	3.657	5.73	4.364	6.181

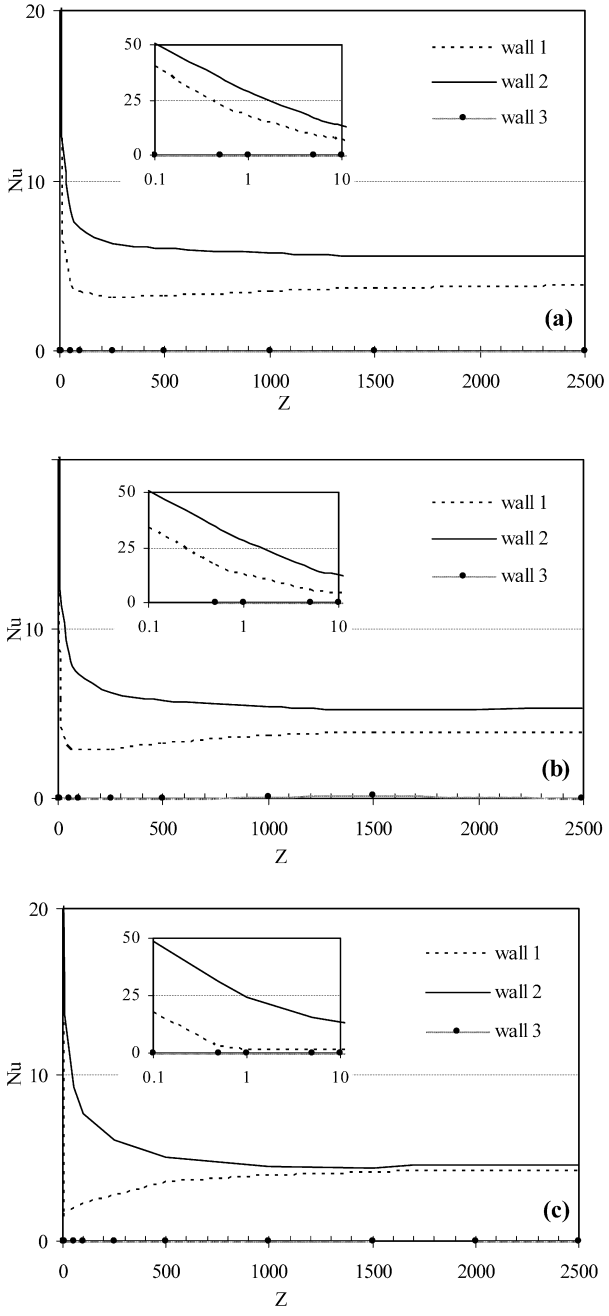

Fig. 8. Axial evolution of the Nusselt number ((a) $Ri_c = 0.34$, (b) $Ri_c = 1$, (c) $Ri_c = 4.85$).

to the corresponding results for forced convection by Shah and London [20].

First we focus on heat transfer between the warm fluid in the cylinder and the wall separating the two fluid streams. In the three cases under consideration the bulk temperature for this fluid decreases uniformly as Z increases. The same is true beyond $Z \geqslant 500$ for the wall temperature. Therefore, as pointed out by Shah and London [20], for these conditions the value of Nu_1 lies between the corresponding values of Nu_T and Nu_H for wall 1; this is also predicted by the present numerical results for mixed convection. Furthermore, as Ri_c decreases, the results of Fig. 7 show that the wall temperature becomes almost uniform. Therefore, Nu_1 decreases approaching Nu_T as Ri_c decreases and it increases tending towards Nu_H when Ri_c increases.

Next we consider heat transfer between the cold fluid in the annulus and the wall separating the two fluids. In the three cases under consideration the former increases monotonically while the latter decreases monotonically beyond $Z \geqslant 500$. For these conditions Shah and London [20] have established that Nu_2 is smaller than Nu_T for wall 2 as predicted by the present numerical results for mixed convection. Furthermore, as Ri_c decreases and the wall temperature becomes almost uniform, Nu_2 increases approaching the corresponding value of Nu_T.

Finally, Fig. 9 shows the axial evolution of the friction coefficient at the three walls. In the upstream adiabatic zone the initial value is always very high since the imposed velocity profile at $Z = -120$ is uniform. Very quickly however, this value decreases and reaches the analytical fully developed values ($f\,Re_1 = 64$, $f\,Re_2 = 111$, $f\,Re_3 = 87.4$). Then as the fluids enter the heat transfer zone, the axial evolution of the friction coefficients reflects the corresponding evolutions of the velocity profiles (cf. Fig. 3). The value at $r = 0.5d_1$ decreases very rapidly and reaches negative values for $Ri_c \geqslant 1$ in the region with flow reversal. The value at $R = 0.5d_2$ decreases slightly towards a minimum value which decreases as Ri_c decreases. On the other hand, the value at $r = 0.5d_3$ increases as Ri_c decreases. Eventually, all three friction coefficient approach asymptotically the corresponding values prevailing in the fully developed region of the upstream adiabatic zone.

5. Conclusion

Laminar mixed convection in a vertical double pipe heat exchanger has been studied by solving the corresponding partial equations numerically. The fluid is a 50% solution of aqueous glycol with temperature dependent viscosity and density. The heat exchanger geometry, the two inlet temperatures and the mass flow rate of the cold fluid in the annulus were held constant while the mass flow rate of the warm fluid in the cylinder was assigned three values. The corresponding Richardson numbers are 0.34, 1 and 4.85.

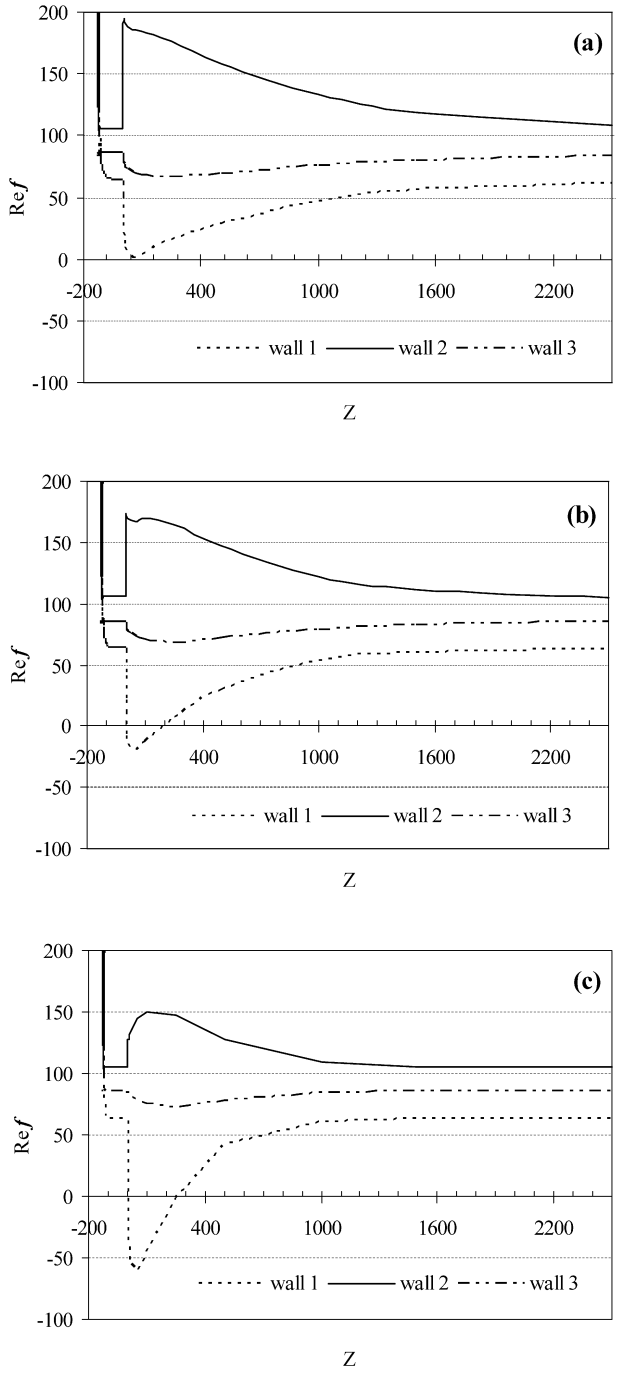

Fig. 9. Axial evolution of the friction factor ((a) $Ri_c = 0.34$, (b) $Ri_c = 1$, (c) $Ri_c = 4.85$).

The results which include temperature and velocity profiles at different cross sections as well as the axial evolution of bulk and wall temperatures, Nusselt numbers and friction factors show that:

- Upstream diffusion in the cylinder modifies the velocity profile at the inlet of the heat transfer region when $Ri_c = 4.85$;
- Flow reversal occurs in the cylinder for $Ri_c \geqslant 1$; the region of negative velocities increases as Ri_c increases;
- For the cases under consideration, the velocity profile and the bulk temperature in the annulus do not vary much since the corresponding mass flow rate is much higher than in the cylinder;
- Near the wall, the temperature of the warm fluid in the cylinder decreases in the direction of flow (increasing Z) when flow reversal is not present; this situation is normal for parallel flow heat exchangers. On the other hand, in the region with flow reversal this temperature increases in the direction of flow (increasing Z); this situation is normal for counterflow heat exchangers;
- The temperature of the wall separating the two streams is almost uniform for $Ri_c = 0.34$; on the other hand, for $Ri_c \geqslant 1$ it exhibit local minimum and maximum values in the entry region which give rise to complex strain and stress situation;
- The local Nusselt number for the warm fluid in the cylinder exhibits a minimum value near the heat exchanger inlet; on the other hand, the local Nusselt number for the cold fluid in the annulus decreases monotonically in the flow direction;
- For the three cases under consideration the asymptotic values of the Nusselt number in the cylinder lie between the corresponding forced convection values for the H and T thermal conditions; on the other hand, in the annulus the asymptotic values of the Nusselt number are always smaller than the corresponding forced convection values for both the H and T thermal conditions;
- The local values of the friction coefficient in the entry region are strongly influenced by the value of the Richardson number; in the developed region they approach asymptotically the corresponding values for forced convection.

All these results clearly indicate that a forced convection model would not be satisfactory for the cases under consideration.

Acknowledgements

The authors thank the “Agence universitaire de la Francophonie – Bureau Europe Centrale et Orientale” and the “Natural Sciences and Engineering Research Council of Canada” for their financial support to the present study.

References

[1] T.M. Hallman, Combined forced and free laminar heat transfer in vertical tubes with uniform heat generation, ASME Trans. 78 (1956) 1831–1841.
[2] Y. Mori, K. Futagami, S. Tokuda, M. Nakamura, Forced convective heat transfer in uniformly heated horizontal tubes, J. Heat Mass Transfer 9 (1966) 453–463.
[3] B. Zeldin, F.W. Schmidt, Developing flow with combined forced–free convection in an isothermal tube, ASME J. Heat Transfer 94 (1972) 211–223.
[4] M. Bernier, B.R. Baliga, Visualization of upward mixed convection flows in vertical pipes using a thin semitransparent gold-film heater and dye injection, Int. J. Heat Fluid Flow 13 (1992) 241–249.
[5] M. Wang, T. Tsuji, Y. Nagano, Mixed convection with reversal flow in the thermal entrance region of horizontal and vertical pipes, Int. J. Heat Mass Transfer 37 (1994) 2305–2319.

[6] G.S. Barozzi, E. Zanchini, M. Mariotti, Experimental investigation of combined forced and free convection in horizontal and inclined tubes, Meccanica 20 (1985) 18–27.

[7] J. Orfi, N. Galanis, C.T. Nguyen, Développement simultané hydrodynamique et thermique d'un écoulement laminaire dans un tube incliné en régime de convection mixte, Revue Générale de Thermique 36 (2) (1997) 83–92.

[8] V. Ianello, K.Y. Suh, N.E. Toderas, Mixed convection friction factors and Nusselt numbers in vertical annular and subchannel geometries, Int. J. Heat Mass Transfer 31 (10) (1988) 2175–2189.

[9] W. Aung, H.E. Mogdaham, F.K. Tsou, Simultaneous hydrodynamic and thermal development in mixed convection in a vertical annulus with fluid property variations, J. Heat Transfer 113 (1991) 926–931.

[10] G. Pagliarini, Steady laminar heat transfer in the entry region of circular tubes with axial diffusion of heat and momentum, Int. J. Heat Mass Transfer 32 (6) (1989) 1037–1052.

[11] H. Nesredine, N. Galanis, C.T. Nguyen, Effects of axial diffusion on laminar heat transfer with low Peclet numbers in the entrance of thin vertical tubes, Numer. Heat Transfer A 33 (1998) 247–266.

[12] P.J. Heggs, D.B. Ingham, D.J. Keen, The effects of heat conduction in the wall on the development of recirculating combined convection flows in vertical tubes, Int. J. Heat Mass Transfer 33 (3) (1990) 517–523.

[13] M. Ouzzane, N. Galanis, Effet de la conduction pariétale et de la répartition du flux thermique sur la convection mixte près de l'entrée d'une conduite inclinée, Int. J. Therm. Sci. 38 (7) (1999) 622–633.

[14] D. Choudhury, S.V. Patankar, Combined forced and free laminar convection in the entrance region of an inclined isothermal tube, ASME J. Heat Transfer 110 (1988) 901–909.

[15] I. Voicu, T. Mare, A.G. Schmidt, C.T. Nguyen, N. Galanis, Numerical and experimental investigation for reverse flow in an isothermal inclined tube, in: International Conference on Thermal Engineering, Beirut, Liban, 2004.

[16] A.D. Carr, M.A. Connor, H.O. Buhr, Velocity, temperature, and turbulent measurements in air for pipe flow with combined free and forced convection, ASME J. Heat Transfer (1973) 445–452.

[17] A. Bezhadmehr, N. Galanis, A. Laneville, Low Reynolds number mixed convection in vertical tubes with uniform heat flux, Int. J. Heat Mass Transfer 46 (2003) 4823–4833.

[18] J.D. Jackson, M.A. Cotton, B.P. Axcell, Studies of mixed convection in vertical tubes: a review, Int. J. Heat Fluid Flow 10 (1) (1989) 2–15.

[19] S. Piva, G.S. Barozzi, M.W. Collins, Combined free and forced convection in horizontal flow: A review, in: Computational Analysis of Convection Heat Transfer, WIT Press, Southampton, 2000, pp. 279–360 (Chapter 8).

[20] R.K. Shah, A.L. London, Laminar Flow Forced Convection in Ducts, Advances in Heat Transfer, Supplement 1, Academic Press, New York, 1978.

[21] S.V. Patankar, Numerical Heat Transfer and Fluid Flow, Hemisphere, McGraw-Hill, New York, 1980.

[22] K.D. Hagen, Heat Transfer with Applications, Prentice-Hall, Upper Saddle River, NJ, 1998, pp. 641–642.

[23] Fluent, Fluent 6 User's Guide, 2002.

[24] S. Kakaç, R.K. Shah, W. Aung, Handbook of Single Phase Convective Heat Transfer, Wiley, New York, 1987.